Modeling of Fe-Based Soft Magnetic Materials for Multiphysical Analysis of Medium-Frequency Transformers

Yang Li, *Member, IEEE*, Zhichao Luo, *Member, IEEE*, Yongjian Li, *Member, IEEE*,
Jianguo Zhu, *Senior Member, IEEE*, Bo Zhang, *Fellow, IEEE*, and Jun Zou

***Abstract*—Fe-based soft magnetic material such as amorphous or nanocrystalline alloy is an alternative to the ferrite for magnetic cores of the medium-frequency transformers (MFTs) due to its high permeability and magnetic saturation. However, accurate core loss modeling is one of the major obstacles to design a high-power-density MFT, especially when considering the nonlinearity hysteresis B-H loop. Besides, the magnetostriction that exhibits hysteresis characteristic causes the vibration issue. Several studies have proven that the high intensity of acoustic noise will do harm to the human's mental and physical health. However, the research on the modeling of the acoustic vibration caused by magnetostriction has been scarcely conducted. In this article, the Jiles–Atherton (J-A) model is applied to describe the hysteresis characteristic of the B-H and H-strain for the Fe-based soft magnetic material. The J-A magnetic and magentomechanical hysteresis models were incorporated into the finite element analysis (FEA) under the multiphysics simulation environment in order to estimate the core loss and temperature rise of the MFT. The acoustic vibration FEA model of the MFT was built based on the H-strain hysteresis J-A model. The fidelity of the simulated acoustic noise pressure was verified by the experiment test results. The proposed models in this article can be effective tools to evaluate the hysteresis magnetic and magnetomechanical behavior of the core in the MFT.**

***Index Terms*—Hysteresis model, magnetomechanical property, medium-frequency transformer, multiphysics analysis.**

NOMENCLATURE

M_{irr}	Irreversible magnetization intensity.
M_{rev}	Reversible magnetization intensity.
M_{an}	Anhysteresis magnetization intensity.
M_s	Saturation magnetization intensity.
H_e	Effective magnetic field intensity.
a	Langevin parameter.
φ	Local field parameter.
k	Pinning parameter.
β	Reversible magnetization coefficient.
f	Excitation frequency.
p_{hys}	Core power loss per unit volume in a period due to the magnetic hysteresis.
p_{eddy}	Eddy current power loss per unit volume.
p_{ex}	Excess power loss per unit volume.
t	Thickness of the material.
κ	Conductivity of the material.
Γ	Euler gamma function.
a_{ex}	Excess power loss coefficient 1.
b_{ex}	Excess power loss coefficient 2.
λ_s	Saturation magnetostriction strain of the material.
$\lambda_{isotropy}$	Magnetostriction strain of the isotropy material.
λ_{an},	Magnetostriction strain of the anhysteresis ideal material.
λ_{irr}	Irreversible magnetostriction strain.
η	Pinning coefficient.
σ	Magnetostriction stress.
a_λ	Magnetostriction correction coefficient 1.
b_λ	Magnetostriction correction coefficient 2.
p	Acoustic pressure.
q	Dipole source.
c_0	Speed of light.
u	Vibration displacement vector in the core.
ρ_0	Density of the medium.
N	Number of the sampling points.
ε_0	Initial strain.
$B_{m,l}$	lth B measurement.
$B_{c,l}$	lth B calculation value.
$B_{m,avg}$	Average value of all the B measurement results.
p_{ref}	Lowest audible amplitude of the sound pressure at 1 kHz.
p_{rms}	RMS value of the sound pressure in one cycle.

I. INTRODUCTION

THE medium-frequency (from several kHz to tens of kHz) transformer is the critical component of the solid-state

Manuscript received 15 November 2023; revised 21 February 2024; accepted 7 April 2024. Date of publication 6 May 2024; date of current version 4 September 2024. This work was supported in part by the National Natural Science Foundation of China under Grant 52130710 and in part by the State Key Laboratory of Power System Operation and Control under Grant SKLD23KM01. *(Corresponding author: Zhichao Luo.)*

Yang Li and Jun Zou are with Tsinghua University, Beijing 100084, China (e-mail: liyang0927@mail.tsinghua.edu.cn; zoujun@tsinghua.edu.cn).

Zhichao Luo and Bo Zhang are with the South China University of Technology, Guangzhou 510640, China (e-mail: hgzcluo@scut.edu.cn; epbzhang@scut.edu.cn).

Yongjian Li is with the Hebei University of Technology, Tianjin 300131, China (e-mail: liyongjian@hebut.edu.cn).

Jianguo Zhu is with The University of Sydney, Sydney, NSW 2006, Australia (e-mail: jianguo.zhu@sydney.edu.au).

This article has supplementary material provided by the authors and color versions of one or more figures available at https://doi.org/10.1109/TPEL.2024.3393241.

Digital Object Identifier 10.1109/TPEL.2024.3393241

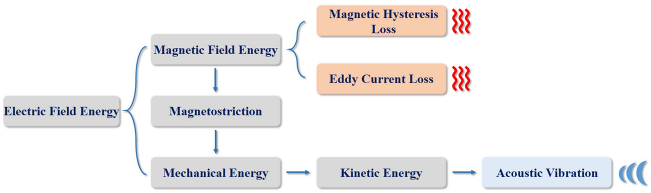

Fig. 1. Schematic of energy flow of the soft magnetic material during magnetization.

transformer which is widely used in the power distribution system [1] and the extremely fast charging infrastructure [2]. Fe-based soft magnetic material such as amorphous or nanocrystalline exhibits its unique advantages over ferrite [3], [4], [5], [6]. The amorphous or nanocrystalline soft magnetic material has a higher permeability and magnetic saturation (up to 1T) and lower core loss when operating at the medium frequency compared to the ferrite counterpart.

However, the core loss estimation remains a main obstacle at the design stage when applying the Fe-based soft magnetic material as a core in the transformer. Fig. 1 presents the energy flow of the Fe-based soft magnetic material during magnetization. The alternating electric field generated by the winding of the medium-frequency transformer (MFT), which can be in a sinusoidal, triangular, or pulsed width modulation manner, will induce an external magnetic field that consequently magnetizes the core. Due to the motion of the magnetic domain wall and the rotation of the domain magnetic moment during the magnetization, the internal magnetization intensity lags behind the external excitation, which is also called magnetic hysteresis [7]. Eddy current loss is caused by the alternating magnetic field inside the core. Besides, when an external magnetic field is applied, the magnetostriction simultaneously occurs in the core along with the magnetic hysteresis. The magnetostriction mechanical energy leads to the vibration of the core which will become a sound wave emitted to the surrounding area.

The magnetic hysteresis and eddy current loss take up the major portion of the core loss. The empirical formulas such as Steinmetz [8] and improved generalized Steinmetz [9] equations are the conventional method to predict the hysteresis and eddy current loss. The Jiles–Atherton (J-A) theory is based on the inhibition of domain wall motion by pinning sites (i.e., inclusions, voids, crystal boundaries, and lattice defects), and is very helpful in describing the behavior of domain wall motion at the primary hysteresis stage [10]. The Preisach model describes the hysteresis phenomenon through an infinite set of magnetic dipoles, which relate to the mechanisms of rotation of aligned moments within a domain [11]. Different from the empirical method, the J-A or Preisach model considers the inherent magnetization mechanism to describe the magnetic hysteresis characteristic of the soft magnetic material and is able to provide a more accurate core loss estimation.

The magnetomechanical property is another important consideration when designing the MFT. The conventional model to evaluate the magnetostriction strain is by interpolating a single-valued function of B-λ or H-λ (λ is the magnetostriction strain) [12], [13]. However, experiment observations have shown that the magnetostriction exhibits hysteresis characteristics in terms of H or B [14], [15]. An accurate magnetostriction model for the soft magnetic material lays a foundation to predict the acoustic noise emission of the MFT. Several previous studies have proven that the medium-frequency acoustic noise is detrimental to the human's auditory ability and mental health [16], [17]. The INIRC/IRPA suggested that the admissible maximum sound pressure level (SPL) should be below 70 dB at 20 kHz and 100 dB at 25–100 kHz [16]. In [18], Villar indicated that the SPL of the MFT made by an amorphous core reaches 100 dB when operating at 2 kHz, 0.48T. In [19], the researchers compared the SPL of the MFT with different soft magnetic cores at 4 kHz, 0.5 T and found that the MFT with the nanocrystalline core has the lowest SPL of 69 dB, which is close to the safety threshold of 70 dB. The key step to simulate the transformer sound field is the computation of the iron core's vibration strain and displacement. In [20], a sine function based on frequency and vibration measurement results is constructed to determine the vibration displacement of the iron core for numerical analysis, and subsequently calculates the distribution of the transformer sound field. However, this method can only achieve a trend analysis of the sound field distribution and cannot provide a precise analysis. On the other hand, in [21], the B-λ curve is utilized to calculate the magnetostriction strain distribution on the iron core based on the magnetic flux density distribution, and then the distribution of the transformer sound field is determined. However, the interpolation of the B-λ curve is only a rough approximation of magnetostriction based on several repeatable experiments. Once the excitation is distorted, the accuracy of the model degrades rapidly. Therefore, an accurate acoustic noise prediction model is crucial for the prevention of the noise safety issue in the MFT design.

Even though the precise hysteresis model is developed, the accurate core loss estimation is still challenging because the magnetic field inside the core is not always homogenously distributed. Therefore, finite element analysis (FEA) is necessary to calculate the magnetic field distribution with a complex core geometry. Normally, in the FEA model, the hysteresis characteristic of the core is not considered and the core loss is approximately estimated by the pure empirical Steinmetz equation limiting the accurate prediction of the core loss [22]. Therefore, it is necessary to consider combining the hysteresis model with the FEA model.

As shown in Fig. 2, the main contributions of this article are as follows.

1) Apply the J-A theory to model the hysteresis characteristic of B-H and λ-H.
2) Incorporate the J-A magnetomechanical models into the FEA model to predict the core loss and acoustic noise for the MFT.

The main goal of this article is to provide power electronics engineers with the knowledge to estimate the core loss and acoustic noise level of the MFT at the transformer design stage.

In Section II, the B-H and λ-H hysteresis models are introduced. Then, in Section III, the detailed procedures of the hysteresis models are explained. In Section IV, the B-H and λ-H hysteresis models are verified by the experiment measurements. The heat and sound pressure distribution models of the MFT are also verified by the experiments.

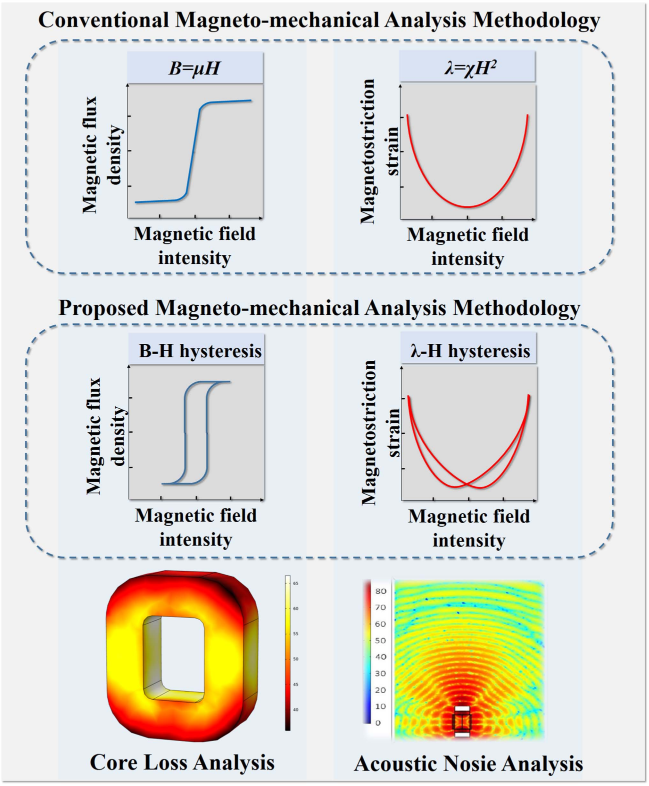

Fig. 2. Schematic of the magnetomechanical analysis methodology.

II. HYSTERESIS MODELS FOR THE FE-BASED SOFT MAGNETIC MATERIAL

A. B-H Hysteresis Model

According to the J-A theory, the magnetization intensity M of soft magnetic material can be divided into two parts: the irreversible magnetization intensity M_{irr} due to the pinning effect and the reversible magnetization intensity M_{rev} due to the elastic bending of the domain wall [23], [24].

In the J-A theory, it assumes that the M-H curve of an ideal material without the pinning effect can be expressed by a single-valued function called anhysteresis function. For the isotropic material, the anhysteresis curve can be simplified as a Langevin function.

$$M_{an} = M_s \left[\coth\left(H_e/a\right) - \left(a/H_e\right)\right] \tag{1}$$

where M_s is the saturation magnetization intensity, and a is the Langevin parameter.

H_e is the effective magnetic field intensity and $H_e = H + \varphi M$. H is the excitation magnetic field intensity and φ is the local field parameter which indicates the coupling among the magnetic domain walls. In the ideal material, $M = M_{an}$.

According to the law of energy conservation, the actual magnetic energy is the subtraction of the magnetic energy of the ideal magnetization and energy loss due to the irreversible magnetization, which can be expressed by

$$\mu_0 \int M dH_e = \mu_0 \int M_{an} dH_e - \mu_0 k\delta \int \left(\frac{dM_{irr}}{dH_e}\right) dH_e \tag{2}$$

where μ_0 is the vacuum permeability, k is the pinning parameter, and δ is the direction function ($\delta = 1$ when $dH/dt \geq 0$, and $\delta = -1$ when $dH/dt < 0$).

Then the following equation can be obtained:

$$M = M_{an} - k\delta \frac{dM_{irr}}{dH_e}. \tag{3}$$

Based on the magnetic domain wall bending theory, the reversible magnetization intensity can be calculated by

$$M_{\text{rev}} = \beta\left(M_{an} - M_{irr}\right) \tag{4}$$

where β is the reversible magnetization coefficient.

Considering the constitutive relation $B = \mu_0(M+H) \approx \mu_0 M$, the core power loss per unit volume in a period due to the static magnetic hysteresis can be calculated by

$$p_{hys} = f \oint H dB. \tag{5}$$

Since the operating frequency of the MFT ranges from several kHz to tens of kHz, the eddy current loss in the Fe-based soft magnetic material is not negligible even though the lamination technique is applied. According to [25], the eddy current power loss per unit volume with the given thickness t can be obtained by

$$p_{eddy} = \frac{t^2\kappa}{12}\left(\frac{dB}{dt}\right)^2 = H_{eddy}\frac{dB}{dt} \tag{6}$$

where κ is the conductivity of the material.

The magnetic field intensity contributed by the eddy current loss can be expressed as follows:

$$H_{eddy} = \frac{t^2\kappa}{12}\frac{dB}{dt}. \tag{7}$$

However, with (7), correction eddy current loss analytical results can be obtained on a very limited frequency bandwidth. In [26], a fractional order derivative of B in (7) is proposed instead of the first-order derivative in order to achieve a better analytical calculation of eddy current loss on a large frequency bandwidth.

The classical form of fractional calculus is given by Riemann, which is expressed as follows:

$${}_{t_0}^{RL}D_t^n f(t) = \frac{d^n f(t)}{dt^n} = \frac{1}{\Gamma(m-n)}\frac{d^n}{dt^n}\int_{t_0}^{t}\frac{f(\tau)}{(t-\tau)^{1+n-m}}d\tau \tag{8}$$

where Γ is the Euler gamma function, $m-1 < n \ll m$, and $m = \lceil n \rceil$.

Therefore, (6) can be modified as follows:

$$p_{eddy} = \frac{t^2\kappa}{12}\frac{d^nB}{dt^n}\frac{dB}{dt} \tag{9}$$

and

$$H_{eddy} = \frac{t^2\kappa}{12}\frac{d^nB}{dt^n} = k_e\frac{d^nB}{dt^n}. \tag{10}$$

Due to the existence of magnetic domains, the local eddy currents are generated near the domain walls when the domain configuration changes under a dynamic excitation, resulting in the excess loss. The excess power loss can be calculated by

$$p_{ex} = k_{ex}(f)\left|\frac{dB}{dt}\right|^{\frac{3}{2}} \tag{11}$$

where $k_{ex}(f) = a_{ex}\, f^{b_{ex}}$ is a function of operating frequency. And

$$H_{ex} = k_{ex}(f)\left|\frac{dB}{dt}\right|^{\frac{1}{2}}. \tag{12}$$

In order to reflect the eddy current loss and excess loss in the B-H loop, the magnetic field intensity can be modified as follows:

$$H_{tot} = H + H_{eddy} + H_{ex}. \tag{13}$$

B. λ-H Hysteresis Model

When an external magnetic field is applied, the magnetostriction occurs along the direction of the external excitation field for the isotropic material. The quadratic domain rotation model was proposed in [27] to describe the relationship between magnetostriction strain λ and magnetization intensity *M*.

$$\lambda = 1.5\lambda_s M^2/M_s^2 \tag{14}$$

where M, M_s, and λ_s are the magnetization intensity, saturation magnetization intensity, and saturation magnetostriction strain of the material, respectively.

According to (14), λ is the single-valued quadratic function of *M*. However, some studies [28], [29] have revealed that there is a hysteresis characteristic between λ and *M* in the power frequency scenario. Therefore, the "butterfly loop" is applied to describe the λ-*M* relationship instead of the parabolic curve.

In order to consider the hysteresis characteristic of λ-*M* operating up to several kHz for MFT applications, the J-A theory is applied in this article. By applying the law of energy conservation, the actual magnetostriction energy in one period is the subtraction of the magnetostriction energy of the anhysteresis magnetostriction and energy loss due to the irreversible magnetostriction, which can be expressed by

$$-\int \sigma d\lambda_{isotropy} = -\left(\int \sigma d\lambda_{an} + \eta \int \sigma d\lambda_{irr}\right) \tag{15}$$

where σ is the magnetostriction stress, $\lambda_{isotropy}$, λ_{an}, and λ_{irr} are the strain of the isotropy material, anhysteresis ideal material, and irreversible magnetostriction, respectively, and η is the pinning coefficient.

By applying (14), (15) can be rewritten as follows:

$$\lambda_{isotropy} = \frac{3}{2}\frac{\lambda_s}{M_s^2}k_\lambda\left(M_{an}^2 + \eta M_{irr}^2\right) = K_\lambda\left(M_{an}^2 + \eta M_{irr}^2\right) \tag{16}$$

where k_λ is the correction function since (14) is applicable to the monocrystalline material and the correction coefficient is needed for the polycrystalline material.

When considering polycrystalline materials, the distribution of magnetic domains cannot be ignored in the influence on magnetostriction. The effective or peak magnetic flux density of the material directly reflects the distribution of magnetic domains, and therefore exhibits a strong correlation with the peak magnetic flux density, presenting a correction parameter that can be described by

$$K_\lambda = a_\lambda\left(1 - \frac{1}{e^{b_\lambda - B_{peak}}}\right) \tag{17}$$

where a_λ and b_λ are the undetermined coefficients.

If the *H-M* relationship is obtained by the discussion in the last subsection, then the λ-*H* hysteresis model can be built using (16).

C. Acoustic Noise Model

The acoustic noise can be evaluated by using the wave equation of the acoustic pressure. By solving the wave equation, the acoustic pressure distribution can be obtained as a function of time and space. In this article, the source of the acoustic noise is the vibration of the core in the MFT. Therefore, in the FEM model, the acoustic pressure field is approximately excited by the dipole source. The acoustic pressure field governing equation can be expressed as follows:

$$\Omega_{air}: \nabla \cdot (\nabla p - q) - \frac{1}{c_0^2}\frac{\partial^2 p}{\partial t^2} = 0 \tag{18}$$

where p is the acoustic pressure, q is the dipole source, and c_0 is the speed of light.

The acoustic pressure field is determined by the magnetostriction strain λ. The mechanical-acoustic boundary coupling condition on the surface of the core is governed by

$$\mathbf{n} \cdot \left[\frac{1}{\rho_0}\nabla \cdot (\nabla p - q)\right] = -\mathbf{n} \cdot \frac{\partial^2 u}{\partial t^2} \tag{19}$$

where u is the vibration displacement vector in the core, ρ_0 is the density of the medium, and $\mathbf{n}$ is the unit vector in the direction of the outward normal.

u can be calculated by using the λ-H hysteresis model discussed in Section II-B.

III. HYSTERESIS MODELS NUMERICAL IMPLEMENTATION

In order to conduct a numerical calculation of the proposed hysteresis models, the iterative method is applied in this article. In this section, the calculation procedures of the B-H, λ-H, σ-λ, and acoustic sound pressure models will be discussed, respectively.

A. B-H and λ-H Hysteresis Models

The time iterative method is applied to conduct the numerical calculation of the B-H and λ-H hysteresis models. This calculation can be run in MATLAB script or incorporated into the FEA model. The idea of this calculation is to obtain the B or λ of a soft magnetic material based on a given H-field excitation. As shown in Fig. 3, the procedures of the numerical calculation of the B-H and λ-H hysteresis models are explained step by step as follows.

Step I: Determine the total sampling points, discretize the H-field excitation in time sequence, and initialize $M(1) = 0$ and $H_e(1) = 0$.

Step II: Calculate the effective H field excitation, H_e, and the anhysteresis magnetization intensity, M_{an} at the time interval i.

Step III: Calculate the differential of M_{irr} based on (3).

Step IV: Calculate the differential of M based on (4) and calculate B according to the constitutive relation. Then $i = i+1$ and repeat the calculation from Step II until $i>N$.

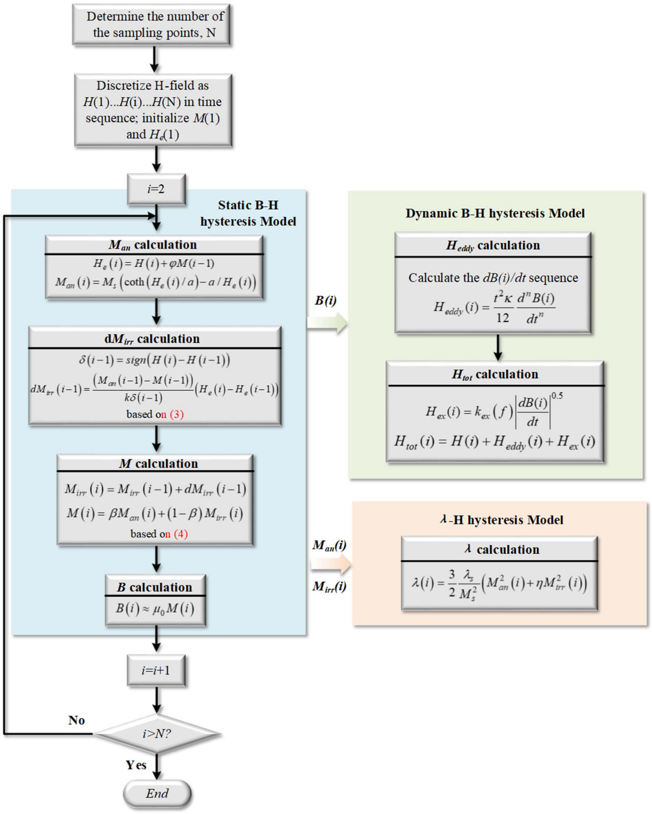

Fig. 3. Flowchart of the numerical calculation of the B-H and λ-H hysteresis models.

Step V: Calculate the first-order derivative of B and then obtain H_{eddy} in (10).

Step VI: Calculate H_{ex} based on (12) and obtain H_{tot} based on (13).

Step VII: Calculate the magnetostriction strain λ based on (16).

B. *Heat Transfer Model*

Thermal analysis is a crucial design consideration to design a reliable MFT [30], [31]. In the heat transfer model, the heat sources are the winding and the core of the MFT. The energy loss in the winding can be regarded as a homogenous heat source. Once the ac resistance of the winding is obtained, the heat rate of the winding is determined. In terms of the ac resistance model of the winding in MFT, several literature proposed an analytical model based on Dowell's theory [32], [33]. Since the main focus of this article is the core loss, the ac winding resistance derivation is not given in detail.

Due to the large time scale difference between the magnetic field model and the heat transfer model, two separate models are built where the magnetic field model is run in a microsecond time scale and the heat transfer model is run in a minute time scale as illustrated in Fig. 4. The procedures to estimate the core temperature of the MFT are listed as follows.

Step I: The "Magnetic fields" is applied in a microsecond time scale incorporating the B-H hysteresis model proposed in Section II-A.

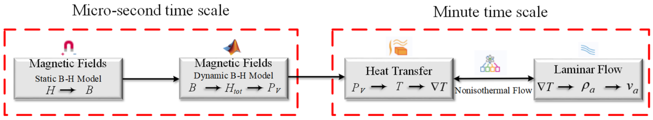

Fig. 4. Flowchart of the heat transfer FEA multiphysics model.

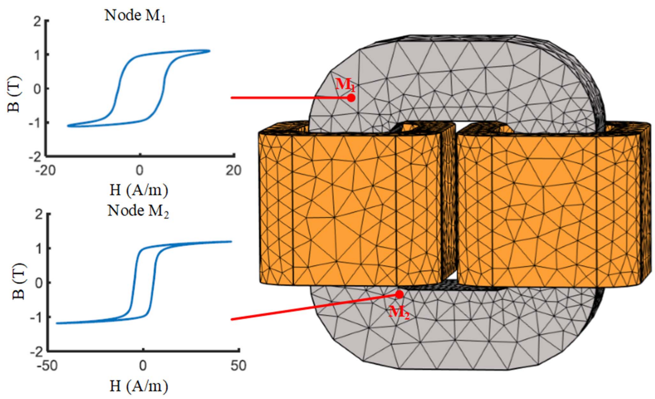

Fig. 5. Core loss density extraction from the magnetic field model.

Step II: As presented in Fig. 5, each node of the core has a unique B-H loop in a period due to the uneven B-field distribution inside the core. Extract the B-field distribution at each node of the core FEM model.

Step III: Calculate the dynamic B-H loop in (10) and (12) according to the B-field distribution obtained by Step II.

Step IV: Calculate the area of the dynamic B-H loops of all nodes. Then the core power loss per volume P_v as a function of the node coordinate *x, y, z* is obtained by interpolation.

Step IV: Apply $P_v(x,y,z)$ as the general heat source in the heat transfer model. For the coil winding, a fixed heat source is applied. Then the gradient of the temperature ∇T can be calculated.

Step V: In order to consider the flow dynamics of the air, the "Laminar Flow" is applied and the "Nonisothermal Flow" boundary is used to build up the connection between the "Heat transfer" and the "Laminar Flow." As such, the air density ρ_a variation and airflow velocity v_a due to the gradient of the temperature is obtained and the natural cooling condition is simulated.

C. *Acoustic Pressure Field Model*

The acoustic pressure field model can be built by incorporating the λ-H hysteresis model into the multiphysics FEA tool, Comsol.

Step I: The "Magnetic fields" is applied in the FEA model. The constitutive relation B-H of the core in the MFT is set as the magnetization model. The differential (3) can be incorporated into the model instead of building the soft magnetic material property. Then the magnetostriction strain can be calculated in (16).

Step II: The "Solid Mechanics" is added to the FEA model in order to build the mechanical vibration model of the core. In

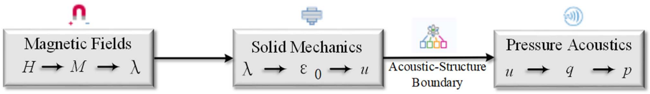

Fig. 6. Flowchart of the acoustic pressure field FEA multiphysics model.

this case, the "linear elastic material" is used and the magnetostriction strain obtained from *Step I* is used as the initial strain ε_0. Then the displacement of the core u is calculated.

Step III: The "Pressure Acoustic (Transient)" is used in the FEA model. The "Acoustic-Structure Boundary" multiphysics interface is added to build up the connection between the "Solid Mechanics" and "Pressure Acoustic (Transient)" governed in (19) as shown in Fig. 6. Then the acoustic pressure field p in the air is calculated in (18).

IV. EXPERIMENT VERIFICATION AND DISCUSSION

In this section, two Fe-based soft magnetic materials, amorphous 1k101 and nanocrystalline 1k107b, are analyzed by using the hysteresis models proposed in Section II. The magnetic and mechanical properties of these two materials are compared and discussed. Furthermore, a scale-downscaled MFT with the nanocrystalline 1k107b core was built to conduct the thermal and acoustic noise tests. The excitation in the simulation and experiment presented in this section is the square wave with a 50% duty cycle.

A. B-H Hysteresis Test

1) Experiment Setup: The experiment setup of the B-H test is presented in Fig. 7. This test rig was used for the Fe–Si steel magnetic property test under alternating and rotational magnetization [34]. As shown in Fig. 7(b), the key component of the test rig is the double-yoke magnetization structure which can provide a two-dimensional excitation to the test sample. The test sample is made of several pieces of the amorphous or nanocrystalline sheet with a dimension of 50 mm × 50 mm stacked up to 1 mm thick. The B-H sensing board shown in Fig. 7(c) is attached tightly to the surface of the test sample. The B-H sensing data are transmitted to the host computer for further analysis. Because the main magnetic flux loop in the MFT is one-dimensional in most of the applications, only one-dimensional B-field excitation is generated by the double-yoke magnetization structure in this article.

2) Model Parameter Identification: As discussed in Section II-A, the B-H hysteresis model has several undetermined parameters listed in Table I. Particle swarm optimization is applied to conduct the parameter identification, where each particle of the swarm is defined as a potential solution for the identification problem in the space. The parameters are optimized by the data acquired by the magnetic property test rig under several specific conditions. This method was validated by some of the previous work [28], [35], [36] where the hysteresis models of the electrical steel sheet at the power frequency were proposed.

Amorphous is characterized by a disordered and noncrystalline structure, where the arrangement of atoms displays irregular quasi-periodicity. In contrast, nanocrystalline has a crystalline structure, but with significantly reduced grain sizes, usually within the nanometer range. This disparity in structure results in variations in magnetic domain structure, magnetic domain wall energy, and magnetic hysteresis behavior between amorphous and nanocrystalline materials. As a result, there are differences of the internal magnetic characteristic parameters between amorphous and nanocrystalline as listed in Tables I and II.

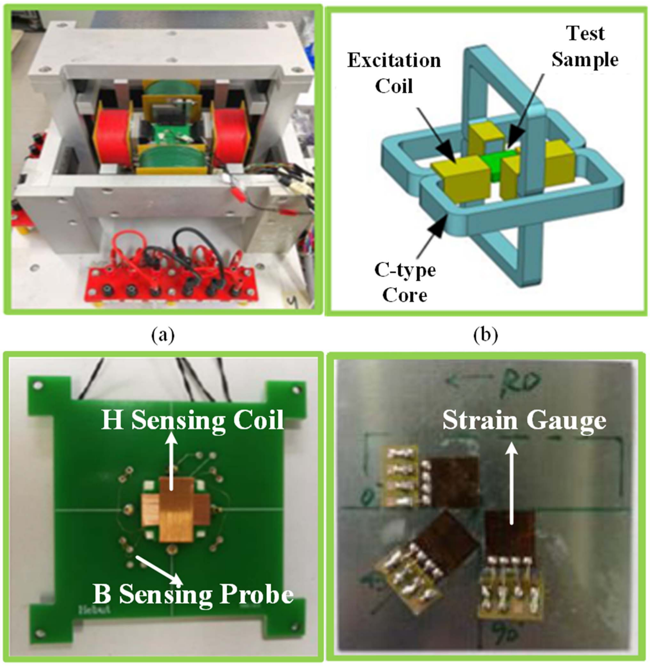

(a) (b)

(c) (d)

Fig. 7. Magnetic property test rig. (a) Overview of the test rig. (b) Double-yoke magnetization structure. (c) B-H sensing board. (d) Rosette foil resistance strain gauges.

TABLE I
B-H HYSTERESIS MODEL PARAMETER IDENTIFICATION

Parameter	Amorphous 1k101	Nanocrystalline 1k107b
Saturation magnetization intensity M_s (A/m)	1.58×10^6	0.89×10^6
Langevin parameter a (A/m)	458	2.2
Local field parameter φ	7.5×10^{-4}	9.6×10^{-5}
Pinning parameter k (A/m)	111	2.88
Reversible magnetization coefficient β	0.88	0.7
Macroeddy current coefficient k_e	2.97×10^{-5}	3.2×10^{-5}
Fractional order n	0.95	0.93
Microeddy current coefficient 1 a_{ex}	0.53	7×10^{-3}
Microeddy current coefficient 2 b_{ex}	–0.17	–0.15

Fig. 8 presents the calculation and experiment results of the B-H curves of the amorphous 1k101 under three different conditions, namely 1T@500 Hz, 1.2T@500 Hz, and 1T@1 kHz. In order to quantitatively analyze the accuracy of the proposed

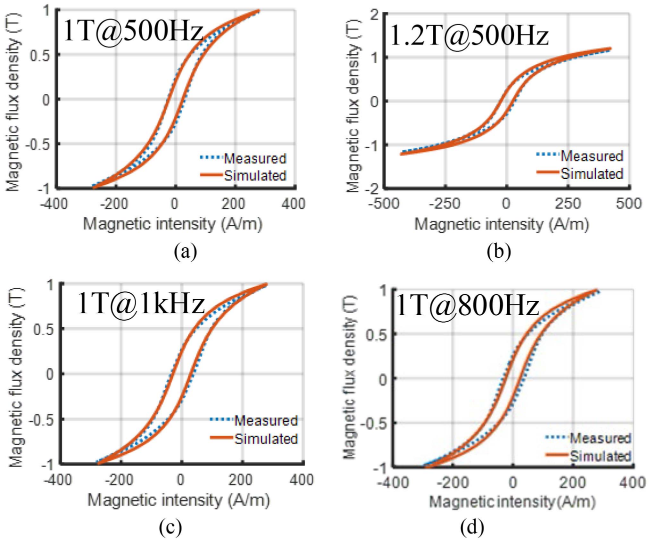

(a) (b) (c) (d)

Fig. 8. B-H experiment results of amorphous 1k101. (a) 500 Hz 1T. (b) 500 Hz 1.2T. (c) 1 kHz 1T. (d) 800Hz 1T. (The simulated results in this figure are obtained by the proposed B-H hysteresis model run in MATLAB).

TABLE II
MAGNETOSTRICTION STRAIN HYSTERESIS MODEL PARAMETER IDENTIFICATION

Parameter	Amorphous 1k101	Nanocrystalline 1k107b
Correction coefficient 1 a_λ	6.87×10^{-18}	4.35×10^{-18}
Correction coefficient 1 b_λ	1.92	1.46
Pinning coefficient η	0.5	0.35

hysteresis models, a curve-fitting evaluation function is applied.

$$R^2 = \frac{\sum_{l=1}^{N}(B_{m,l} - B_{m,ave})^2 - \sum_{l=1}^{N}(B_{m,l} - B_{c,l})^2}{\sum_{l=1}^{N}(B_{m,l} - B_{m,ave})^2} \tag{20}$$

where N is the total number of the measurement points, $B_{m,l}$ is the lth B measurement, $B_{c,l}$ is the lth B calculation value, and $B_{m,avg}$ is the average value of all the B measurement results.

3) Experiment Results Analysis: R^2 is in a range of [0, 1]. The R^2 closer to 1 is the better the curve fitting is. As shown in Fig. 8, the calculated results show good agreement with the experiment measurement. The maximum core loss density error is 4.9% as listed in Table III. As the frequency increases to 1 kHz, the peak magnetic flux density in the amorphous is limited to 1T due to the demagnetizing field generated by the eddy current. Compared the core loss density per cycle under two different conditions (1T@500 Hz and 1 T@1 kHz), it can be seen that as the frequency increases from 500 Hz to 1 kHz, the core loss density per cycle has a 28% increase (from 9.38 to 12.021 mW/kg/cycle) due to the eddy current loss. In order to verify the generalization ability of the proposed method, the B-H loop under 1T@800 Hz (not used as the data set in the parameter identification) is measured in the experiment test rig and compared with the calculation from the J-A model as shown in Fig. 8(d). The predicted core loss is 10.82 W/kg and the measured core loss is 10.98 W/kg, indicating that the proposed method is able to predict the BH loop under excitation conditions other than the parameter identification data set with high accuracy.

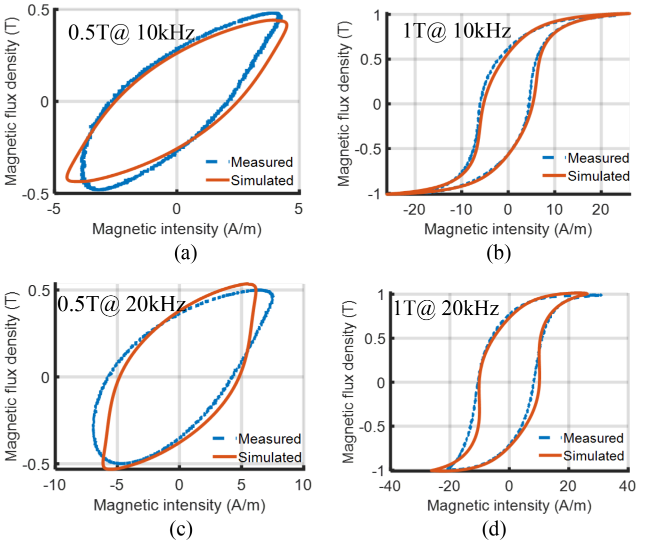

(a) (b) (c) (d)

Fig. 9. B-H experiment results of nanocrystalline 1k107b. (a) 10 kHz 0.5T. (b) 10 kHz 1T. (c) 20 kHz 0.5T. (d) 20 kHz 1T. (The simulated results in this figure are obtained by the proposed B-H hysteresis model run in MATLAB).

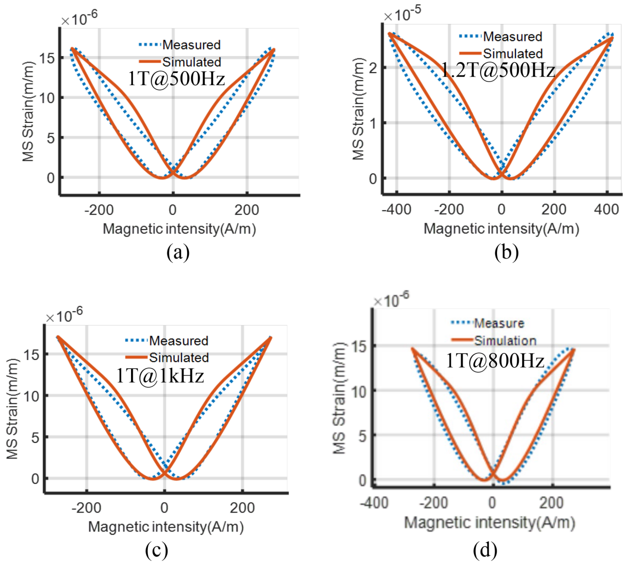

(a) (b) (c) (d)

Fig. 10. λ-H experiment results of amorphous 1k101. (a) 500 Hz 1T. (b) 500 Hz 1.2T. (c) 1 kHz 1T. (d) 800 Hz 1T. (The simulated results in this figure are obtained by the proposed λ-H hysteresis model run in MATLAB).

The experiment results of the nanocrystalline 1k107b under 10 and 20 kHz in Fig. 9. The maximum relative error between the calculated and experiment results is −5.7% as listed in Table IV. The curve fitting evaluation function R^2 is higher than 0.98 in all the studied cases, which suggests that the hysteresis model can predict the B-H constitutive relation of the nanocrystalline at the medium frequency accurately. The core loss density per cycle increases by 40.4% (from 1.39 to 1.96 mW/kg/cycle) when the operating frequency increases from 10 to 20 kHz. The portion of loss increase is mainly due to the eddy current loss in the

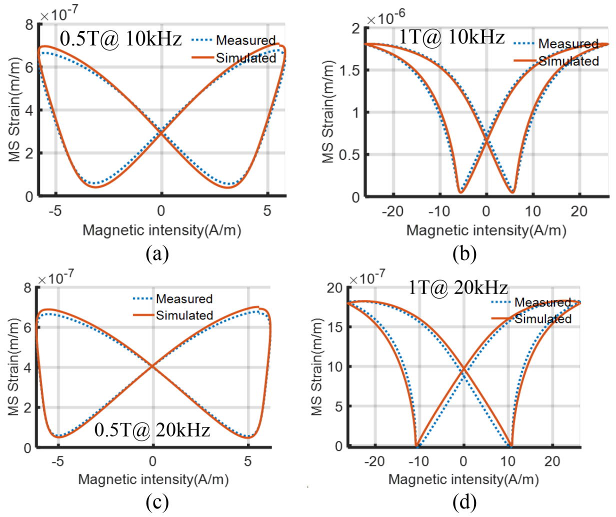

(a) (b) (c) (d)

Fig. 11. λ-H experiment results of nanocrystalline 1k107b. (a) 10 kHz 0.5T. (b) 10 kHz 1T. (c) 20 kHz 0.5T. (d) 20 kHz 1T. (The simulated results in this figure are obtained by the proposed λ-H hysteresis model run in MATLAB).

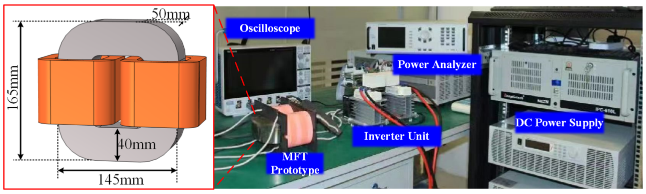

Fig. 12. Schematic of the nanocrystalline transformer.

TABLE III
COMPARISON BETWEEN CALCULATED AND MEASURED RESULTS OF 1K101

Excitation condition	Measured loss density (W/kg)	Calculated loss density (W/kg)	Relative error (%)	R^2 of B-H curve fitting
1T@500Hz	4.690	4.783	2.0	0.995
1.2T@500Hz	5.431	5.552	2.2	0.993
1T@1kHz	12.021	12.620	4.9	0.991
1T@800Hz	10.982	10.825	1.4	0.995

TABLE IV
COMPARISON BETWEEN CALCULATED AND MEASURED RESULTS OF 1K107B

Excitation condition	Measured loss density (W/kg)	Calculated loss density (W/kg)	Relative error (%)	R^2 of B-H curve fitting
0.5T@10kHz	7.086	6.702	−5.73	0.990
1T@10kHz	21.261	23.821	12.04	0.976
0.5T@20kHz	21.748	21.988	1.09	0.997
1T@20kHz	88.912	95.365	6.77	0.993

TABLE V
CALCULATED AND MEASURED RESULTS COMPARISON OF 1K101

Excitation condition	Average relative error (%)	R^2 of λ-H curve fitting
1T@500Hz	5.4	0.984
1.2T@500Hz	5.2	0.983
1T@1kHz	3.2	0.990
1T@800Hz	2.9	0.991

TABLE VI
CALCULATED AND MEASURED RESULTS COMPARISON OF 1K107B

Excitation condition	Average relative error (%)	R^2 of λ-H curve fitting
0.5T@10kHz	4.2	0.988
1T@10kHz	1.9	0.997
0.5T@20kHz	2.6	0.995
1.0T@20kHz	3.9	0.989

nanocrystalline and it will become more dominant in the core loss as the frequency increases.

Compared with the core loss data shown in Tables III and IV, the core loss density per cycle of the nanocrystalline 1k107b is 2.126mW/kg/cycle in the 1T@10 kHz case while the one of the amorphous 1k101 is 12.021mW/kg/cycle in the in the 1T@1kHz case. This suggests that the nanocrystalline 1k107b is more suitable for MFTs operating at tens of kHz.

B. λ-H Hysteresis Test

In the λ-H hysteresis test, the double-yoke magnetization structure shown in Fig. 7 is applied and several strain gauges are attached closely to the surface of the material to obtain the magnetostriction strain as shown in Fig. 7(d). Only one-dimensional magnetostriction strain along the B-field excitation is measured in this test.

In this test, the λ-H hysteresis characteristic of both amorphous 1k101 and nanocrystalline 1k107b is studied. In Fig. 10, the λ-H hysteresis butterfly loop is presented under 500 Hz and 1 kHz sinusoidal excitations. The peak strain at 500 Hz, 1T is 14.7 μm/m and reaches 21.7 μm/m when the peak magnetic flux density is 1.2T. The curve fitting evaluation function and the relative error are listed in Table V. The R^2 of the λ-H hysteresis loop is higher than 0.983 and the maximum average relative error is less than 5.4%. The λ-H loop under 1T@800 Hz (not used as the data set in the parameter identification) is measured in the experiment test rig and compared with the calculation from the J-A model as shown in Fig. 10(d). The proposed method based on the J-A theory can predict the λ-H loop with high accuracy under the condition that is not used in the parameter identification data set.

The λ-H butterfly loops of the nanocrystalline 1k107b are displayed in Fig. 11. The calculated results and experiment measurement are quantitatively compared as listed in Table VI. It can be seen that the calculated butterfly loops of all excitations match the experiment measurement well. The maximum average relative error is less than 3.3%. By comparing Fig. 11(a), (c), and (e), it is interesting to note that the frequency has a minor effect on the maximum magnetostriction strain. However, it has a considerable effect on the shape of the butterfly loop. The higher the frequency is, the more obvious a hysteresis loop can be observed. This closely relates to the magnetomechanical damping loss and will be discussed in the next subsection.

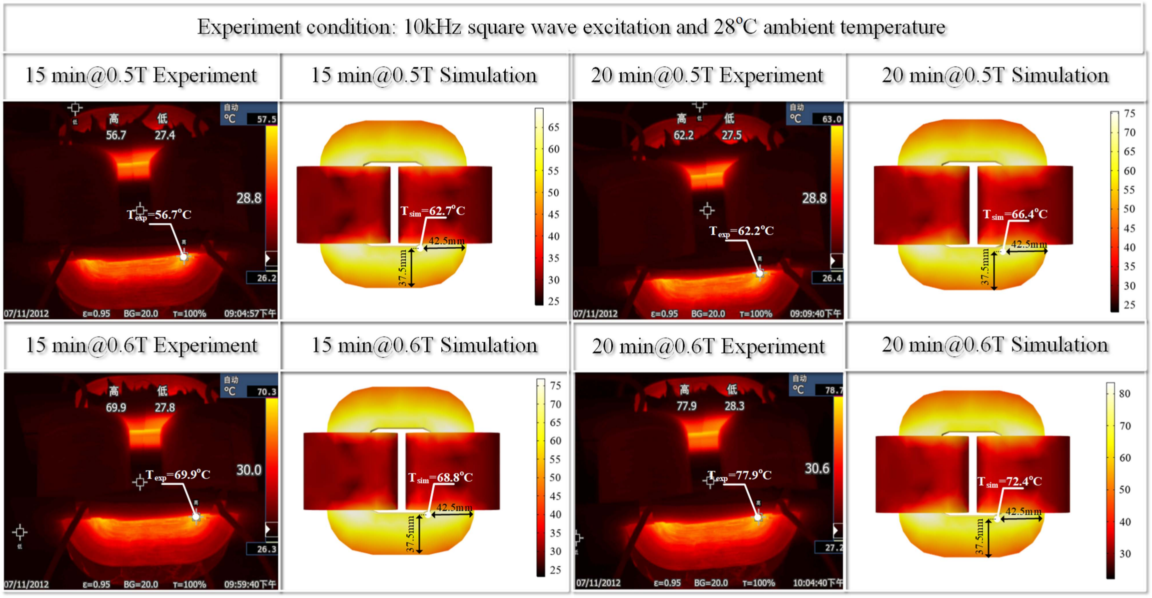

Fig. 13. Heat run simulation and experiment results.

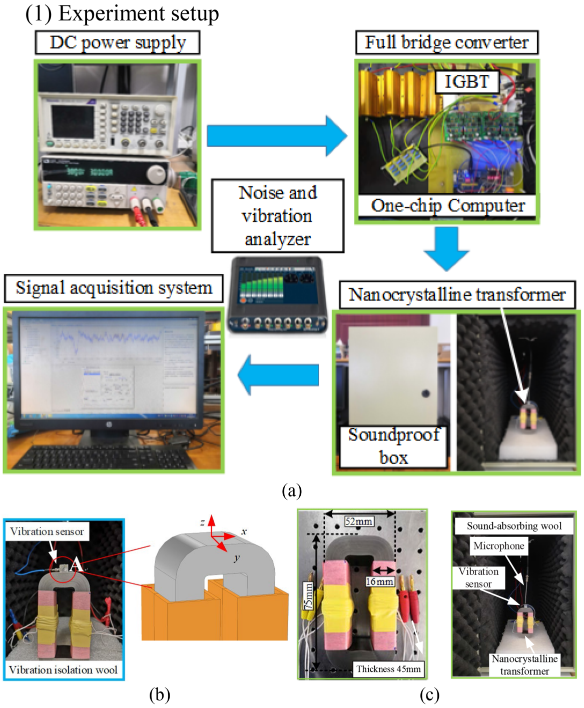

(a)

(b)

(c)

Fig. 14. Experiment setup of the acoustic noise test. (a) Vibration and acoustic noise test platform. (b) Sensor in the vibration test. (c) Transformer prototype and the setting of the acoustic noise test.

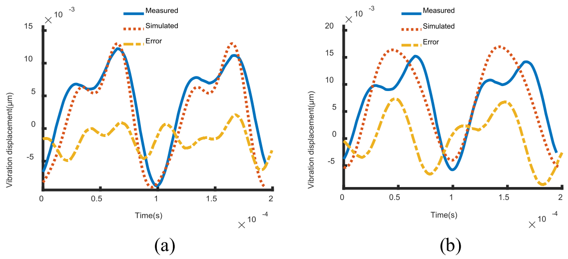

(a)

(b)

Fig. 15. Comparison between the simulation and experiment results of the vibration displacement at the reference point A. (a) Proposed hysteresis model. (b) Conventional model.

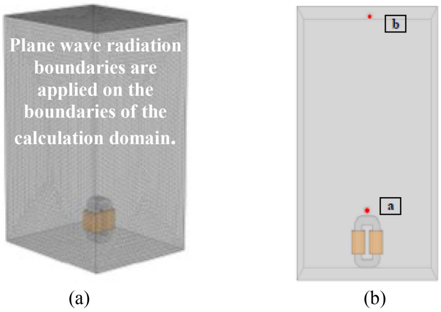

(a)

(b)

Fig. 16. Acoustic noise FEA model. (a) Overview of the FEA model. (b) Acoustic noise test points.

C. *Temperature Rise Test*

In order to verify the multiphysics simulation model incorporating the B-H dynamic hysteresis characteristic, a transformer prototype made of a nanocrystalline core 1K107b was built in the lab, which is shown in Fig. 12. In the heat transfer simulation model, the thermal conductivity of 1k107b in the lamination direction is 0.71 W/(m•K), while the thermal conductivity in the other two directions is 18 W/(m•K). The specific heat capacity of the nanocrystalline is set as a constant value of 288 J/(kg•K). The emissivity value of the 1K107b is 0.2. In [37], it is reported that the core loss density and the magnetic saturation of the Fe-based nanocrystalline are stable when the operating temperature of the core is under 100°C. Therefore, the magnetic properties of

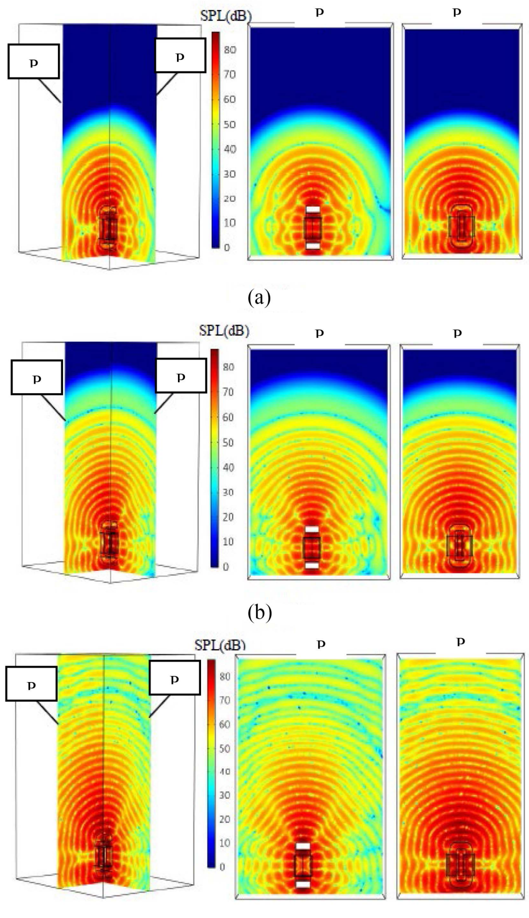

(a)

(b)

(c)

Fig. 17. Acoustic pressure field around the MFT prototype at different time intervals in the FEA model. (a) t = 0.4 ms. (b) t = 0.7 ms. (c) t = 1.5 ms.

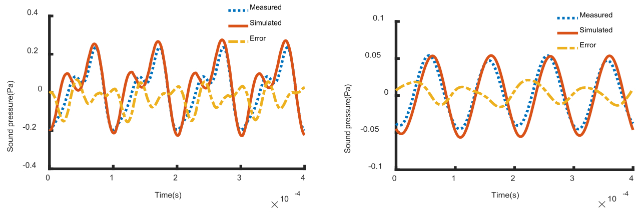

(a) (b)

Fig. 18. Comparison between the calculated and experiment results of the acoustic noise pressure. (a) Reference point a. (b) Reference point b.

the core material are fixed in the heat transfer model. In order to simulate the heat transfer dynamic environment, the bottom surface of the computational region in the simulation is assigned a wall boundary condition, while the other five surfaces are assigned open boundary conditions. This is well aligned with the experiment condition as shown in Fig. 12.

The number of turns of the transformer is 11 and the primary side is excited by the full-bridge inverter while the secondary side is open-circuit. The nanocrystalline core was run under 0.5T@10 kHz or 0.6T @10 kHz for 20 min and the ambient temperature was 28°C. The simulation and experiment results are shown in Fig. 13. The maximum estimation error of the simulation results is 9.5%, which suggests that the proposed FEM model incorporating the dynamic B-H hysteresis characteristic is a useful reference to predict the core temperature on the design stage.

In order to verify the effectiveness and accuracy of the multiphysics FEA simulation model, a vibration and acoustic noise test platform was built as shown in Fig. 14. The test platform includes a dc power source from ITECH, a full-bridge inverter, a Yokogawa PX8000 power analyzer, a SQuadrigalI vibration and noise recorder from HEAD acoustics GmbH, a microphone and a soundproof chamber. The background noise inside the soundproof chamber is 21.1 dB. During the test, a 5 kHz, 80 V square wave excitation is provided by the full-bridge inverter. A scale-down MFT prototype was built as shown in Fig. 14(c). The number of turns of the core winding is 6. Then the vibration of the core and the acoustic noise in the surrounding area are measured and compared to the FEA simulation.

D. *Acoustic Noise Test*

1) *Experiment Setup:*

a) Vibration Test: As presented in Fig. 14(b), a 3-axis vibration sensor is attached to point A at the top of the core. The bandwidth of the sensor is 10 MHz. The hysteresis FEA simulation results are compared with the experiment measurement in Fig. 15(a). The average relative error is 11.2%. The conventional FEA simulation (apply the conventional single-valued function constitutive relation as shown in Fig. 2) results are also compared to the experiment measurement as shown in Fig. 15(b). The average relative error is 26.7%. It can be seen that the conventional FEA model cannot reflect the high-order harmonics of the vibration displacement.

2) Acoustic Noise Test: The FEA acoustic noise simulation model is presented in Fig. 16(a). The calculation domain for the acoustic field is established as a rectangular cuboid based on the dimensions of the soundproof box. Given that the interior walls of the soundproof box are all lined with sound-absorbing cotton, plane wave radiation boundaries are implemented around the perimeter, as well as at the bottom and top of the calculation domain, to ensure that no echoes impact the acoustic field calculation. The SPL at the reference points a and b is studied and compared to the experiment measurement. The SPL is defined by the following equation:

$$SPL\,(dB) = 20\log_{10}\left(\frac{p_{rms}}{p_{ref}}\right) \tag{21}$$

where $p_{ref} = 20\ \mu$Pa, which is the lowest audible amplitude of the sound pressure at 1 kHz, and p_{rms} is the RMS value of the sound pressure in one cycle at the measured point.

The acoustic pressure field at different time intervals from the FEA simulation is presented in Fig. 17. Two perpendicular measurement planes P1 and P2 are investigated to present the acoustic pressure distribution. When t = 0.4 ms, the SPL inside the core window reaches 79.32 dB and the SPL in the vicinity of the core is 73.21 dB. At t = 0.7 ms, the acoustic pressure field radiates to the 4/5 of the chamber. At t = 1.5 ms, the acoustic pressure field has spread throughout the entire area of the soundproof chamber and the SPL at the top of the chamber is 58.08 dB.

The noise pressure at reference points a and b from the FEA simulation is compared to the experiment measurement in Fig. 18(a) and (b). It is interesting to observe that the noise pressure has a high-order harmonic at point a and becomes more sinusoidal at point b. This reveals that the high-order acoustic noise decays faster than the fundamental component when transmitting through the air. The average relative error at point a is 16.2% and is 14.1% at point b, which is acceptable for predicting the acoustic noise distribution around the MFT.

The sound wave propagation video is also uploaded along with the manuscript to provide a better illustration of the sound wave distribution.

V. CONCLUSION

In this article, the multiphysics modeling and analysis of the Fe-based soft magnetic material, namely amorphous 1k101 and nanocrystalline 1k107b, in the MFT are discussed. The dynamic J-A hysteresis model considering the eddy current and excess loss is introduced by applying the concept of the fractional calculus. The multitimescale electromagnetic-thermal model for the estimation of temperature rise in the MFT core is discussed. The J-A hysteresis theory is also applied to the λ-H hysteresis model. The magnetostriction obtained from the λ-H hysteresis model is used as the source of the acoustic noise simulation to predict the SPL in the surrounding area. The detailed multiphysics modeling procedures are presented by using the FEA tool Comsol and the numerical calculation software such as MATLAB.

Since the model includes physical mechanisms, it exhibits strong generalization ability. Once the parameters are determined, the model can provide accurate results under practical operating conditions such as square wave, sine wave excitation, and dc bias without the need for further parameter fitting.

All the multiphysics models introduced in this article are verified by various experimental setups such as the double-yoke magnetization test rig, the thermal experiment platform, and the sound pressure measurement environment chamber. The magnetomechanical properties of two soft magnetic materials are analyzed and compared. The experiment results agree with the results from the numerical calculation or simulation well, which indicates that the proposed models in this article can be effective tools for evaluating the magnetic and magnetomechanical hysteresis behavior of the core in the MFT.

REFERENCES

[1] S. Xu, A. Q. Huang, and R. Burgos, “Review of solid-state transformer technologies and their application in power distribution systems,” *IEEE J. Emerg. Sel. Topics Power Electron.*, vol. 1, no. 3, pp. 186–198, Sep. 2013.

[2] H. Tu, H. Feng, S. Srdic, and S. Lukic, “Extreme fast charging of electric vehicles: A technology overview,” *IEEE Trans. Transp. Electrific.*, vol. 5, no. 4, pp. 861–878, Dec. 2019.

[3] Z. Luo, Y. Zhao, M. Xiong, X. Wei, and H. Dai, “A self-tuning LCC/LCC system based on switch-controlled capacitors for constant-power wireless electric vehicle charging,” *IEEE Trans. Ind. Electron.*, vol. 70, no. 1, pp. 709–720, Jan. 2023.

[4] W. Tong, R. Sun, S. Li, and R. Tang, “Loss and thermal analysis for high-speed amorphous metal PMSMs using 3-D electromagnetic-thermal bi-directional coupling,” *IEEE Trans. Energy Convers.*, vol. 36, no. 4, pp. 2839–2849, Dec. 2021.

[5] Z. Luo, X. Li, C. Jiang, Z. Li, and T. Long, “Permeability-adjustable nanocrystalline flake ribbon in customized high-frequency magnetic components,” *IEEE Trans. Power Electron.*, vol. 39, no. 3, pp. 3477–3485, Mar. 2024.

[6] L. Xiong et al., “IMU-based automated vehicle body sideslip angle and attitude estimation aided by GNSS using parallel adaptive Kalman filters,” *IEEE Trans. Veh. Technol.*, vol. 69, no. 10, pp. 10668–10680, Oct. 2020.

[7] B. D. Cullity and C. D. Graham, *Introduction to Magnetic Materials Second Edition*, Hoboken, NJ, USA: Wiley, 2009.

[8] C. P. Steinmetz, “On the law of hysteresis,” *Proc. IEEE*, vol. 72, no. 2, pp. 197–221, Feb. 1984.

[9] H. Zhao, C. Ragusa, C. Appino, O. de la Barrière, Y. Wang, and F. Fiorillo, “Energy losses in soft magnetic materials under symmetric and asymmetric induction waveforms,” *IEEE Trans. Power Electron.*, vol. 34, no. 3, pp. 2655–2665, Mar. 2019.

[10] D. C. Jiles and D. L. Atherton, “Theory of ferromagnetic hysteresis,” *J. Magnetism Magn. Mater.*, vol. 61, pp. 48–60, 1986.

[11] S. Y. R. Hui and J. Zhu, “Magnetic hysteresis modeling and simulation using the Preisach theory and TLM technique,” in *Proc. Power Electron. Specialist Conf.*, 1994, pp. 837–842.

[12] L. Zhu et al., “Electromagnetic vibration of controllable saturable reactor under different DC control current,” *Int. J. Appl. Electromagn. Mechanics*, vol. 55, pp. 217–227, 2017.

[13] Y. Zhang, J. Wang, X. Sun, B. Bai, and D. Xie, “Measurement and modeling of anisotropic magnetostriction characteristic of grain-oriented silicon steel sheet under DC bias,” *IEEE Trans. Magn.*, vol. 50, no. 2, Feb. 2014, Art. no. 7008804.

[14] M. J. Sablik and D. C. Jiles, “A model for hysteresis in magnetostriction,” *J. Appl. Phys.*, vol. 64, no. 10, pp. 5402–5404, 1988.

[15] A. J. Moses, P. I. Anderson, and S. Somkun, “Modeling 2-D magnetostriction in nonoriented electrical steels using a simple magnetic domain model,” *IEEE Trans. Magn.*, vol. 51, no. 5, May 2015, Art. no. 6000407.

[16] D. d. l. Protection, “Interim guidelines on limits of human exposure to airborne ultrasound,” *Health Phys.*, vol. 46, pp. 969–974, 1984.

[17] M. D. Fletcher et al., “Effects of very high-frequency sound and ultrasound on humans. Part I: Adverse symptoms after exposure to audible very-high frequency sound,” *J. Acoustical Soc. Amer.*, vol. 144, 2018, pp. 2511–2520.

[18] I. Villar, “Multiphysical characterization of medium-frequency power electronic transformers,” Swiss Federal Institute of Technology Lausanne, Lausanne, Switzerland, 2010.

[19] P. Shuai and J. Biela, “Influence of material properties and geometric shape of magnetic cores on acoustic noise emission of medium-frequency transformers,” *IEEE Trans. Power Electron.*, vol. 32, no. 10, pp. 7916–7931, Oct. 2017.

[20] Y. Du, S. Liu, and C. Qiao, “Vibration and noise analysis of power transformers with different rated capacity,” presented at the Int. Conf. Power Syst. Technol., 2023, pp. 1–5.

[21] L. Zhu, J. Hao, and L. Lu, “Research on influence of damping on the vibration noise of transformer,” *IEEE Access*, vol. 10, pp. 92128–92136, 2022.

[22] M. Luo, D. Dujic, and J. Allmeling, “Modeling frequency-dependent core loss of ferrite materials using permeance–capacitance analogy for system-level circuit simulations,” *IEEE Trans. Power Electron.*, vol. 34, no. 4, pp. 3658–3676, Apr. 2019.

[23] Z. Li et al., “Queries on the JA modeling theory of the magnetization process in ferromagnets and proposed correction method,” *Proc. CSEE*, vol. 31, pp. 124–131, 2011.

[24] D. C. Jiles, J. B. Thoelke, and M. K. Devine, “Numerical determination of hysteresis parameters for the modeling of magnetic properties using the theory of ferromagnetic hysteresis,” *IEEE Trans. Magn.*, vol. 28, no. 1, pp. 27–35, Jan. 1992.

[25] B. Ducharne et al., “Dynamics of magnetic field penetration into soft ferromagnets,” *J. Appl. Phys.*, vol. 117, 2015, Art. no. 24.

[26] B. Zhang, B. Gupta, B. Ducharne, G. Sébald, and T. Uchimoto, “Dynamic magnetic scalar hysteresis lump model based on Jiles–Atherton quasi-static hysteresis model extended with dynamic fractional derivative contribution,” *IEEE Trans. Magn.*, vol. 54, no. 11, Nov. 2018, Art. no. 7301605.

[27] D. Jiles, *Introduction to Magnetism and Magnetic Materials*. Boca Raton, FL, USA: CRC Press, 2015.

[28] Z. Lihua, L. Jingjing, Y. Qingxin, Z. Jianguo, and C. S. Koh, “An improved magnetostriction model for electrical steel sheet based on Jiles–Atherton model,” *IEEE Trans. Magn.*, vol. 56, no. 3, Mar. 2020, Art. no. 7514604.

[29] H. Chen, L. Li, and Y. Wang, “Inverse magnetostriction model of electrical steel sheet under DC bias based on energetic and improved Jiles–Atherton–Sablik models,” in *Proc. IEEE 20th Biennial Conf. Electromagn. Field Computation*, 2022, pp. 1–2.

[30] H. Wang, Q. Yang, Y. Li, J. Wang, and Y. Zhao, "Numerical calculation and experimental verification for leakage magnetic field and temperature rise of transformer core tie-plate," *IEEE Trans. Appl. Supercond.*, vol. 29, no. 2, Mar. 2019, Art. no. 0602405.

[31] H. Wang et al., "Thermal design consideration of medium voltage high frequency transformers," in *Proc. IEEE Appl. Power Electron. Conf. Expo.*, 2020, pp. 2721–2726.

[32] P. Dowell, "Effects of eddy currents in transformer windings," in *Proc. Inst. Elect. Engineers*, 1966, pp. 1387–1394.

[33] C. R. Sullivan and R. Y. Zhang, "Analytical model for effects of twisting on litz-wire losses," in *Proc. IEEE 15th Workshop Control Model. Power Electron.*, 2014, pp. 1–10.

[34] S. Yue, Y. Li, Q. Yang, K. Zhang, and C. Zhang, "Comprehensive investigation of magnetic properties for Fe–Si steel under alternating and rotational magnetizations up to kilohertz range," *IEEE Trans. Magn.*, vol. 55, no. 7, Jul. 2019, Art. no. 6100705.

[35] Y. Li, L. Zhu, and J. Zhu, "Core loss calculation based on finite-element method with Jiles–Atherton dynamic hysteresis model," *IEEE Trans. Magn.*, vol. 54, no. 3, Mar. 2018, Art. no. 1300105.

[36] Z. Nemeth and M. Kuczmann, "Measuring and simulating magnetic characteristics using Epstein frame," *Pollack Periodica*, vol. 13, pp. 15–26, 2018.

[37] Z. Luo, X. Li, C. Jiang, and T. Long, "Characterization of nanocrystalline flake ribbon for high frequency magnetic cores," *IEEE Trans. Power Electron.*, vol. 37, no. 12, pp. 14011–14016, Dec. 2022.

Yang Li (Member, IEEE) was born in Hebei, China, in 1992. He received the B.E. degree in electrical engineering and automation from the Hebei University of Technology City College, Tianjin, China, in 2015, the M.E. degree in control engineering from Tiangong University, Tianjin, China, in 2018, and the Ph.D. degree in electrical engineering from the University of Hebei University of Technology, Tianjin, China, in 2022.

He is currently a Postdoctoral Fellow with the Department of Electrical Engineering, Tsinghua University, Beijing, China. His research interests include computational electromagnetics, measurement and modeling of magnetic properties of materials, electrical machines, and power electronics.

Zhichao Luo (Member, IEEE) received the B.S. degree in automotive engineering from the South China University of Technology, Guangzhou, China, in 2014, and the Ph.D. degree in automotive engineering from Tongji University, Shanghai, China, in 2019.

From 2019 to 2021, he was a Postdoctoral Fellow with the Department of Electrical and Computer Engineering, University of Toronto, Canada. From 2021 to 2023, he worked as a Postdoctoral Research Associate with the University of Cambridge, U.K. In 2023, he joined the School of Electric Power Engineering, South China University of Technology, where he is currently an Associate Professor. He has also served as the Industry Liaison Chair of the TC9: Wireless Power Transfer Systems in IEEE Power Electronics Society. His current research interests include wireless power transfer technologies, high frequency magnetic components, novel soft magnetic material, magnetic field modeling, and power electronics in electric vehicles.

Yongjian Li (Member, IEEE) was born in Hebei, China, in 1978. He received the B.E., M.E., and Ph.D. degrees in electrical engineering from the Hebei University of Technology (HEBUT), Tianjin, China, in 2002, 2007, and 2011, respectively.

From 2009 to 2011, he was an Assistant Professor in electromagnetic with the University of Technology Sydney, Australia. From 2016 to 2017, he was a Visiting Scholar with Ottawa University, Ottawa, ON, Canada. In 2002, he joined HEBUT, where he is currently a Professor in electromagnetic with the School of Electrical Engineering and also the Deputy Director of the State Key Laboratory of Reliability and Intelligence of Electrical Equipment. His research interests include the measurement of magnetic properties, modeling of magnetic materials, and power electronics.

Jianguo Zhu (Senior Member, IEEE) received the B.E. degree from Jiangsu Institute of Technology, Jiangsu, China, in 1982, the M.E. degree from Shanghai University of Technology, Shanghai, China, in 1987, and the Ph.D. degree from the University of Technology Sydney (UTS), Sydney, NSW, Australia, in 1995, all in electrical engineering.

In 1994, he was appointed a Lecturer with UTS, promoted to full professor in 2004, and a Distinguished Professor of Electrical Engineering in 2017. At UTS, he has held various leadership positions, including the Head of School for the School of Electrical, Mechanical, and Mechatronic Systems and the Director of the Centre for Electrical Machines and Power Electronics. In 2018, he joined the School of Electrical and Information Engineering, The University of Sydney (USyd), Sydney, NSW, Australia, as the Head of the School and a Full Professor. After completing his term as the Head of School in 2023, he is currently a Full Professor with USyd. His research interests include computational electromagnetics, measurement and modeling of electromagnetic properties of materials, electrical machines and drives, power electronics, renewable energy systems, and smart grids.

Bo Zhang (Fellow, IEEE) was born in Shanghai, China, in 1962. He received the B.S. degree in electrical engineering from Zhejiang University, Hangzhou, China, in 1982, the M.S. degree in power electronics from Southwest Jiaotong University, Chengdu, China, in 1988, and the Ph.D. degree in power electronics from the Nanjing University of Aeronautics and Astronautics, Nanjing, China, in 1994.

He is currently a Professor of the School of Electric Power, South China University of Technology, Guangzhou, China. He has authored or coauthored more than 600 papers and held more than 230 patents. He has authored nine monographs. His research interests include nonlinear analysis and control of power electronics, wireless power transfer technology, and ac drives.

Jun Zou was born in Wuhan, Hubei, China, in 1971. He received the B.S. and M.S. degrees from Zhengzhou University, Zhengzhou, China, in 1994 and 1997, respectively, and the Ph.D. degree from Tsinghua University, Beijing, China, in 2001, all in electrical engineering.

In 2001, he joined the Electrical Engineering Department, Tsinghua University, as an Assistant Researcher. In 2011, he was promoted to be a Professor. His research interests include EMC in power systems and computational electromagnetics.